DR LEI LI (Orcid ID : 0000-0002-6794-8459)
DR XIAO QIANG LIU (Orcid ID : 0000-0001-8028-0644)
PROFESSOR XIANG MING CHEN (Orcid ID : 0000-0001-7029-0662)

Article type : Article

Structure and microwave dielectric characteristics of $Sr_2[Ti_{1-x}(Al_{0.5}Nb_{0.5})_x]O_4$ ($x \leq 0.50$) ceramics

Iqra Hameed, Shu Ya Wu, Lei Li, Xiao Qiang Liu and Xiang Ming Chen[1]

School of Materials Science and Engineering, Zhejiang University, Hangzhou 310027, China

Abstract

$Sr_2[Ti_{1-x}(Al_{0.5}Nb_{0.5})_x]O_4$ (x=0, 0.10, 0.25, 0.30, 0.5) ceramics were synthesized by a standard solid state reaction process. $Sr_2[Ti_{1-x}(Al_{0.5}Nb_{0.5})_x]O_4$ solid solutions with tetragonal Ruddlesdon-Popper (R-P) structure in space group *I*4/mmm were obtained within $x \leq 0.50$, and only minor amount (1-2wt%) of $Sr_3Ti_2O_7$ secondary phase was detected for the compositions $x \geq 0.25$. The temperature coefficient of resonant frequency τ_f of $Sr_2[Ti_{1-x}(Al_{0.5}Nb_{0.5})_x]O_4$ ceramics was significantly improved from 132 ppm/°C to 14 ppm/ °C correlated with the increase in degree of covalency (%) with increasing *x*. The dielectric constant ε_r decreased linearly with increasing *x*, while high *Qf* value was maintained though it decreased firstly. The variation tendency of *Qf* value was dependent on the trend of packing fraction combined with the microstructure. Good combination of microwave dielectric properties was achieved for *x*=0.50: ε_r =25.1, *Qf* = 77,580 GHz, τ_f =14 ppm/ °C. The present ceramics could be expected as new candidates of ultra-high Q microwave dielectric materials without noble element such as Ta.

---

[1] Corresponding author, E-mail: xmchen59@zju.edu.cn

This article has been accepted for publication and undergone full peer review but has not been through the copyediting, typesetting, pagination and proofreading process, which may lead to differences between this version and the Version of Record. Please cite this article as doi: 10.1111/jace.16510

1.Introduction

A massive development in the field of microwave dielectric ceramics has been explored in the recent years because of their productive applications in microwave communication especially wireless communication systems[1]. In the upcoming technology, the mobile phone communication system will be pursued by 5G technology rather than 3G/4G. The forthcoming 5G technology would require the fastest communication speed and small time delay for the wireless devices, and therefore the microwave dielectric materials with a dielectric constant ranged 20-60 are generally required, in which the ultra-high *Qf* value and the near zero temperature coefficient are also necessary for enhancing the device functionality[2, 3, 4].

Latterly, a number of new compounds with Ruddlesdon- Popper (R-P) structure have attracted immense attention due to their flexible structural characteristics and exceptional dielectric properties[5, 6]. Wise et al.[7, 8] first reported the microwave dielectric characteristics of $Sr_{n+1}Ti_nO_{3n+1}$ (n=1,2,3…∞) R-P compounds, but they did not get high *Qf* value. Recently, Liu et al. [9] reported the ultra-high *Qf* value (145,200 GHz) together with a dielectric constant ε_r= 42 in $Sr_{n+1}Ti_nO_{3n+1}$ (n=1,2) ceramics, while a large positive τ_f (130 ppm/^{o}C) was remained as a big issue. If the τ_f could be improved into an acceptable level, $Sr_{n+1}Ti_nO_{3n+1}$ (n=1,2) ceramics should be the promising new candidates of ultra-high Q microwave dielectric materials without noble element such as Ta.

In the previous work, τ_f of Sr_2TiO_4 ceramics was tuned to 119 ppm/^{o}C, along with the higher *Qf* value (93,550 GHz) and suitable dielectric constant of 39.3 through Ca-substitution for Sr, and the improvement in τ_f was associated to the increased B-site bond valance[10]. Therefore, the authors are still in an urge to further modify $Sr_{n+1}Ti_nO_{3n+1}$ (n=1,2,3…∞) ceramics with R-

P structure to achieve the near-zero τ_f for practical application. It was suggested by some researchers to substitute a combination of acceptor and donor ions at Ti-site, which could consequently improve the microstructure as well as the dielectric properties by restraining the reduction of Ti^{4+} into Ti^{3+} in titanates[11], and co-substitution of $(Al_{0.5}Nb_{0.5})^{4+}$ for Ti^{4+} indicated significant effects in $SrTiO_3$ ceramics.[12] Therefore, it should be an interesting issue to investigate the effects of $(Al_{0.5}Nb_{0.5})$-substitution for Ti in Sr_2TiO_4 ceramics. Because τ_f is strongly dependent upon the structural characteristics of oxygen octahedra such as bond length, bond strength (s), and degree of covalency (%) between the octahedral cation-oxygen ions[13, 14, 15], the significant improvement in τ_f is expected by such co-substitution.

In the present work, $Sr_2[Ti_{1-x}(Al_{0.5}Nb_{0.5})_x]O_4$ (x=0, 0.10, 0.25, 0.30, 0.5) ceramics are synthesized, and the correlation between their microwave dielectric properties and structural characteristics are determined and discussed, for searching the ultra-high *Qf* dielectric ceramics with the near-zero τ_f.

2. Experimental procedures

$Sr_2[Ti_{1-x}(Al_{0.5}Nb_{0.5})_x]O_4$ (x=0, 0.10, 0.25, 0.30, 0.5) ceramics were synthesized by a standard solid state reaction process, using high purity powders of $SrCO_3$ (99.95%), Al_2O_3 (99.99%), Nb_2O_5 (99.95%) and TiO_2 (99.99%) as raw materials. These raw powders were weighed according to their stoichiometric ratios and mixed by ball-milling with ZrO_2 media in alcohol for 24 hours. After drying, the powders with different compositions were calcinated separately at the temperature ranged 1200-1300 °C in air for 3 hours. The calcinated powders were re-milled for 24 hours to get better homogeneity and then dried. Afterwards 4wt% solution of PVA (polyvinyl alcohol) was added into the powders during the granulating process, and then the powders were pressed into the pellets with 12 mm diameter and 2-6 mm thickness under a pressure of 120 MPa. Finally, all the samples were sintered at 1550-1600 °C in air for 3 hours to yield the dense ceramics, and they were cooled down at a rate of 1°C/min to 1000 °C and further cooled inside the furnace.

The bulk density of the ceramics sintered at different temperatures was evaluated by Archimedes method. The crystal structure was determined using X-Ray diffractrometer (XRD) (BRUKER D8 Advance, Germany) using CuKα radiations, and the precious structural analyses was conducted by the Rietveld refinement. The microstructures of the thermally etched surfaces were observed through scanning electron microscopy (SEM) (S-3400; Hitachi, Tokyo, Japan), where the samples were finely polished and later thermally etched at 50°C temperature lower than their actual sintering temperatures for 30 minutes. The dielectric properties of $Sr_2[Ti_{1-x}(Al_{0.5}Nb_{0.5})_x]O_4$ (x=0, 0.10, 0.25, 0.30, 0.5) ceramics were evaluated at microwave frequencies by a vector network analyzer (E8363B, Agilent Technologies Inc., Santa Clara, CA). The dielectric constant ε_r and temperature coefficient of resonant frequency τ_f were measured by Hakki-Coleman method[16], and τ_f was calculated by the following formula:

$$\tau_f = \frac{f_{80}-f_{20}}{(80-20)(f_{20})} \times 10^6 \qquad (1)$$

where, f_{80} and f_{20} were the resonant frequencies at 80 °C and 20 °C, respectively. The Qf was evaluated by the resonant-cavity method[17], by means of a silver-coated cavity linked with network analyzer. As the Q-factor holds inverse relationship with frequency (f) in microwave range, the product of Qf was used despite only Q, to evaluate the dielectric loss.

3. Results and discussions

Fig 1. shows the XRD patterns of $Sr_2[Ti_{1-x}(Al_{0.5}Nb_{0.5})_x]O_4$ ceramics sintered at 1575 °C for 3 hours. The solid solutions with tetragonal R-P structure are identified throughout the compositions, and all the reflection peaks are marked with their relevant crystallographic indices planes of Sr_2TiO_4 (indexed as JCPD card 39-1471) in *I*4/ mmm space group. There is no apparent peak for secondary phase in the XRD patterns. However a very minor amount (1-2wt %) of $Sr_3Ti_2O_7$ (JCPD card 89-1383) secondary phase was detected for the composition $x \geq 0.25$ from the Rietveld analysis (see Fig 2.). In fact, a combination of R-P phases can always be found in the end member ($SrTiO_3$) having excess SrO layers[18, 19], and the real reason for the appearance of $Sr_3Ti_2O_7$ R-P phase can be well explained by the reaction energies. Since the difference between the reaction energies of these R-P phases such as Sr_2TiO_4 (n=1) and $Sr_3Ti_2O_7$ (n=2) is very small, and it subsequently leads to the coexistence of different metastable phases in the sintered ceramics. Therefore, for excess SrO compositions, appearance of $Sr_3Ti_2O_7$ is dynamically favorable.[20, 21].

All the diffraction peaks for Sr_2TiO_4 phase, are actually shifted a little towards the higher 2θ angle. This is related to the small average ionic radius of $(Al_{0.5}Nb_{0.5})^{4+}$ (0.586 Å CN=6) compared with that of Ti^{4+} (0.605 Å CN=6).[22] Fig 2 depicts the Rietveld refinement results of XRD patterns for $Sr_2[Ti_{1-x}(Al_{0.5}Nb_{0.5})_x]O_4$ (x=0, 0.10 and 0.25) ceramics, and the structural parameters for all the compositions are provided in Table 1. The lattice parameters for $Sr_2[Ti_{1-x}(Al_{0.5}Nb_{0.5})_x]O_4$ ceramics, a and c, increase almost linearly with increasing x (see Fig 3). A small decline at x=0.30 is observed for both a and c which again increases at x=0.50, and this is well consistent with Fig2. which indicates the appearance of $Sr_3Ti_2O_7$ secondary phase for $x \geq 0.25$.

The relative density for $Sr_2[Ti_{1-x}(Al_{0.5}Nb_{0.5})_x]O_4$ ceramics as a function of sintering temperature is shown in Fig 4. All ceramics are well densified at 1575 °C -1600 °C, and the bulk density over 98% T.D. (theoretical density) is reached. Also, $(Al_{0.5}Nb_{0.5})$-substitution for Ti obviously reduces the densification temperature of Sr_2TiO_4 ceramics, and densification temperature for compositions with higher x is lower than that for x=0 and 0.1.

Fig 5. shows the microstructures of thermal etched surfaces for $Sr_2[Ti_{1-x}(Al_{0.5}Nb_{0.5})_x]O_4$ ceramics. Dense ceramics are obtained for all compositions, and the microstructure is sensitive to the composition. The samples used for SEM observation are sintered at 1600°C for x=0 and x=0.10 and are sintered at 1575 °C for $x \geq 0.25$. For the composition of x=0, the average grain size is comparatively larger than all other samples. For x=0.10, however, overall grains with obvious inhomogeneity are observed. With further increasing x, the grain size turns out to be more uniformly distinct and elongated in the morphology.

The microwave dielectric characteristics of $Sr_2[Ti_{1-x}(Al_{0.5}Nb_{0.5})_x]O_4$ ceramics are listed in Table 2, where ceramics with the highest densities have been adoped as the samples. The dielectric constant ε_r decreases linearly from ε_r=42 to ε_r =25.1 as a function of x. The temperature coefficient at resonance frequency τ_f is significantly improved from τ_f=132ppm/°C to 14 ppm/°C with increasing x from x=0 to x=0.50. Whereas Qf follows a nonlinear trend with respect to x. At first, Qf decreases from 11, 2900 GHz (at x=0) to 60,200 GHz (at x=0.10), but it arouses sharply to 11,3000 (GHz) at x=0.25, and finally an acceptable high value of 77,580GHz is obtained at x=0.50, where the best τ_f is achieved.

Fig.6 displays the linear relationship between dielectric constant ε_r and theoretical dielectric polarizabilities $\alpha_{Theo.}$(Å^3)$_.$ of $Sr_2[Ti_{1-x}(Al_{0.5}Nb_{0.5})_x]O_4$ ceramics as a function of x. The dielectric constant is persistently reduced by increasing the co-substitution of Al/Nb at B-site. Generally, at microwave frequencies the dielectric constant is dependent upon several factors such as relative density, structural characteristics of the oxygen octahedron in the unit cell i.e. distortion, rattling effect, and tilting[23]. In the present situation, ε_r is dominated by the smaller dielectric polarizability. The theoretical dielectric polarizabilities α_{Theo}(Å^3) have been calculated by the additive rule proposed by Shannon[24] and the corresponding relation could be described as following:

$$\alpha_{theo}(Sr_2[Ti_{1-x}(Al_{0.5}Nb_{0.5})_x]O_4)=\alpha(Sr^{2+})+(1-x)\alpha(Ti^{4+})+0.5x\alpha(Al^{3+})+0.5x\alpha(Nb^{5+})+4\alpha(O^{2-}) \quad (2)$$

where, $\alpha(Sr^{2+})$, $\alpha(Ti^{4+})$, $\alpha(Al^{3+})$, $\alpha(Nb^{5+})$ and $\alpha(O^{2-})$ are the ionic polarizabilities of respective ions specified in equation (2). As shown in Fig.7, one can see that α_{Theo}(Å^3) decreases linearly with the increase in $(Al_{0.5}Nb_{0.5})^{4+}$ content because of the smaller ionic polarizability of $(Al_{0.5}Nb_{0.5})^{4+}$ (2.38 Å^3) than that of Ti^{4+} (2.94 Å^3)[25]. The calculated dielectric constant $\varepsilon_{r\,calc}$ can be evaluated by Clausius Mossoti relation with the aid of dielectric polarizabilities. The Clausius Mossoti equation can be inscribed as follows:

$$\boldsymbol{\alpha_D = \frac{3V_m}{4\pi}\frac{(\varepsilon_r-1)}{(\varepsilon_r+1)}} \qquad (3)$$

where, α_D is the dielectric polarizability calculated by using Equation (2), V_m represents the molecular volume. With increasing x, the dielectric constant ε_r, theoretical dielectric polarizability α_{Theo}(Å^3) and calculated dielectric constant $\varepsilon_{rcalc.}$ of $Sr_2[Ti_{1-x}(Al_{0.5}Nb_{0.5})_x]O_4$

ceramics decrease linearly (see Table 3). Therefore, the trend of dielectric constant as a function of x, is in agreement with the decreasing trend of dielectric polarizability. The synchronized variation tendency of the respected values of ε_r, $\alpha_{Theo.}$(Å^3) and $\varepsilon_{r\ calc}$ can be attributed to the lack of rattling effect in the bond characteristics of oxygen octahedron[14, 26], which is explained in later section.

To validate the formation of stable perovskite structure or stable layered perovskite structure, the basic precondition should have the tolerance factor (t) and electronegativity difference (Δe) equivalent or greater than 0.80 and 1.465, respectively[27]. The tolerance factor provides the approximation of structure stability whereas the electronegativity difference (Δe) expresses the amount of excess binding energy existing between A and B site atoms. Greater the difference (Δe), higher the stability of the structure.[28]

The tolerance factor (t) for $Sr_2[Ti_{1-x}(Al_{0.5}Nb_{0.5})_x]O_4$ ceramics was calculated by using following equation: [29]

$$t = \frac{r_{Sr^{2+}} + r_{O^{2-}}}{\sqrt{2}(r_B + r_{O^{2-}})} \qquad (4)$$

and

$$r_B = (1\text{-}x)\, r_{Ti^{4+}} + x\,(0.5 r_{Al^{3+}}{}^{+} + 0.5 r_{Nb^{5+}}) \qquad (5)$$

where, $r_{Sr^{2+}}$, $r_{O^{2-}}$, $r_{Ti^{4+}}$, $r_{Al^{3+}}$, and $r_{Nb^{5+}}$ are the effective ionic radii of Sr^{2+}, O^{2-}, Ti^{4+}, Al^{3+} and Nb^{5+}, respectively. Fig.7 shows the tolerance factor as a function of x. The value of t rises linearly with increase in x value. This increasing trend of tolerance factor indicates a stable R-P structure throughout all the compositions (see Table 1) which eventually refers to the improved dielectric characteristics. The electronegativity difference (Δe) suggested by Pauling[30] can be calculated as follows:

$$\Delta e=\frac{X_{A-O}+X_{B-O}}{2} \qquad (6)$$

where, $X_{A\text{-}O}$ and $X_{B\text{-}O}$ is the electronegativity difference between A and B-site cation and oxygen ion, respectively. In the present work, both conditions are satisfied as $t>0.95$ and $\Delta e>2$ for $Sr_2[Ti_{1-x}(Al_{0.5}Nb_{0.5})_x]O_4$ ceramics. The bond characteristics of $Sr_2[Ti_{1-x}(Al_{0.5}Nb_{0.5})_x]O_4$ ceramics can be assessed by the degree of covalency (%) which can be calculated through the correlation between bond strength (s) and covalency (f_c) presented in Equation (7)-(9) as following[31, 32]:

$$s=\left(\frac{R}{R_1}\right)^{-N} \qquad (7)$$

$$f_c=as^M \qquad (8)$$

$$\text{Degree of covalency (\%)} = \frac{fc}{s}\times 100 \qquad (9)$$

where, R is the refined average bond length (from the Rietveld refinement data), R_1 and N denotes the empirical constants that rely on the cation site and are these different for each octahedral cation – O^{-2} ion pair. In addition, a and M in Eq. (8) are also the empirical constants depending on the number of electrons.[31] Table 4 sums up the bond strength and average covalency (%) of $Sr_2[Ti_{1-x}(Al_{0.5}Nb_{0.5})_x]O_4$ ceramics. Fig.8 shows the correlation between τ_f and average degree of covalency (%) for $Sr_2[Ti_{1-x}(Al_{0.5}Nb_{0.5})_x]O_4$ ceramics as a function of x. The temperature coefficient of resonance frequency τ_f is significantly improved from 132 ppm/°C to 14 ppm/ °C with increasing x from x=0 to x=0.50. It is obvious that the temperature coefficient of resonance frequency is closely associated with the structural characteristics of oxygen octahedra specifically bond strength, bond valance, degree of covalency (%), rattling effect and secondary phase[15, 33, 34]. Therefore, it is important to relate this decrease in τ_f with the increase in bond strength, lower rattling effect between B-site and oxygen. The bond strength and the degree of covalency (%) between oxygen and B-Site cation turns stronger with increase in the co-substitution of Al/Nb at B-site which consequently decreases τ_f. It has been reported that the higher degree of covalency (%) leads to have stronger covalent bonds than the ionic bonds among cation and oxygen in oxygen octahera and also the increasing trend in bond strength (*s*) signifies to have higher stability of crystal structure by the effect of lower vibration restoring force[13, 35, 36]. These results are in well agreement with not only the higher degree of covalency but also the decreasing trend of dielectric constant for x≤0.50 as discussed above. The rattling effect is strongly dependent on the high bond strength between the cation and oxygen ion in the oxygen octahedron since it generates more rigid octahedra which could decrease the rattling effect and consequently decreases the dielectric constant[37].

Fig. 9 shows the relation between *Qf* value and packing fraction (P.F) for $Sr_2[Ti_{1-x}(Al_{0.5}Nb_{0.5})_x]O_4$ ceramics as a function of *x*. While, Table 5 shows the calculated values of *Qf* and packing fractions for all the compositions. For the composition with *x*=0.10, the *Qf* value drops abruptly from 11,2900 GHz to 60,200 GHz. As the value of *x* increases to *x*=0.25, the *Qf* value sharply increases to 11,3000 GHz. Afterwards, by increasing the co-substitution of $(Al_{0.5}Nb_{0.5})^{4+}$ further the *Qf* value starts to diminish for the other compositions. It is pondered that there are many factors that could possibly affect the *Qf* which are divided into intrinsic and extrinsic ones. Intrinsic loss is affected by the minimum loss linked with lattice anharmonicity which is determined by the specific crystal structure and composition of materials. Whereas, extrinsic loss is affected by lattice defects, secondary phase, porosity, gain size, density, or impurity[38]. In the present case, for *x*=0.10 the sudden decrease *Qf* value is due to decrease in the grain size which ultimately increases grain boundaries where a possible concentration of defects, impurities and large inner stresses are located. Concerned with the intrinsic loss, the decreasing trend of *Qf* is well consistent with the packing fraction as shown in Fig. 9. The packing fraction is measured by the given formula (10):

$$\mathrm{P.F}=\frac{Volume\ of\ atoms\ in\ the\ cell}{Volume\ of\ unit\ cell}\times Z \qquad (10)$$

where, Z=2 (No. of formula units per unit cell). With increasing *x*, the packing fraction decreases linearly from 59.23% to 59.14% as demonstrated (see Table 5). In contrast, at *x*=0.25 the *Qf* increases significantly and it is larger than the *Qf* values measured for other compositions. This could be attributed to the low extrinsic loss dominated by the comparatively larger grain size and homogenous morphology. With further increasing *x*, the *Qf* starts decreasing to 83,960 GHz and 77,580 GHz at *x*=0.30 and *x*=0.50, respectively. This has been already correlated with the decreasing trend of packing fraction[26, 34].

Some typical microwave dielectric ceramics with the dielectric constant close to the present ones are summarized in Table 6. The present ceramics, without noble element such as Ta, indicate the excellent microwave dielectric characteristics which are almost comparable with those of $Ba(Zn_{1/3}Ta_{2/3})O_3$ and $Ba(Mg_{1/3}Ta_{2/3})O_3$ and obviously better than other materials previously reported.

4. Conclusion

Solid solutions with tetragonal Ruddlesdon-Popper (R-P) structure were obtained in $Sr_2[Ti_{1-x}(Al_{0.5}Nb_{0.5})_x]O_4$ ceramics with x≤0.50. The τ_f value was productively tuned to near-zero from 132 ppm/°C to 14 ppm/ °C correlated with the increase in degree of covalency (%) with increasing *x*. The dielectric constant decreased linearly with the increase in co-substitution of Al/Nb in accordance with the ionic polarizabilities, while high *Qf* value was maintained though it decreased firstly. Good combination of microwave dielectric properties was achieved for *x*=0.50 ceramics: ε_r =25.1, *Qf* = 77,580 (GHz), τ_f =14 ppm/ °C. The *Qf* value is expected to be further improved through reducing the imhomogeneity, and then the present ceramics could be expected as new candidates of ultra-high Q microwave dielectric materials without noble elements such as Ta.

Acknowledgements

This work was supported by the Ministry of Science and Technology of China under grant number 2015CB654601.

References

1. Reaney IM, Iddles D. Microwave dielectric ceramics for resonators and filters in mobile phone networks. J Am Ceram Soc.2006;89:2063-2072.

2. Zhou D, Pang LX, Wang DW, Li C, Jin B, Reaney IM. High permittivity and low loss microwave dielectrics suitable for 5G resonators and low temperature co-fired ceramic architecture. J Mater Chem C.2017;5:10094-98.

3. Zhou D, Pang LX, Wang DW, Reaney IM. $BiVO_4$ based high k microwave dielectric materials: a review. J Mater Chem C.2018;6:9290-313.

4. Pang LX, Zhou D. Modification of $NdNbO_4$ microwave dielectric ceramic by Bi substitutions. J Am Ceram Soc. 2018;102:2278–2282.

5. Chen XM, Xiao Y, Liu XQ, Hu X. $SrLnAlO_4$ (Ln=Nd and Sm) microwave dielectric ceramics. J Electroceram.2003;10:111-115.

6. Kamba S, Samoukhina P, Kadlec F, Pokorny J, Petzelt J, Reaney IM, et al. Composition dependence of the lattice vibrations in $Sr_{n+1}Ti_nO_{3n+1}$ Ruddlesden-Popper homologous series. J Eur Ceram Soc.2003;23:2639-45.

7. Wise PL, Reaney IM, Lee WE, Price TJ, Iddles DM, Cannell DS. Structure-microwave property relations of Ca and Sr titanates. J Eur Ceram Soc.2001;21:2629-32.

8. Wise PL, Reaney IM, Lee WE, Price TJ, Iddles DM, Cannell DS. Structure–microwave property relations in $(Sr_xCa_{(1-x)})_{n+1}Ti_nO_{3n+1}$. J Eur Ceram Soc.2001;21:1723-26.

9. Liu B, Li L, Liu XQ, Chen XM. $Sr_{n+1}Ti_nO_{3n+1}$ (n=1, 2) microwave dielectric ceramics with medium dielectric constant and ultra-low dielectric loss. J Am Ceram Soc.2016;100:496-500.

10. Hameed I, Liu B, Li L, Liu XQ, Chen XM. $(Sr_{1-x}Ca_x)_2TiO_4$ microwave dielectric ceramics with R-P structure (x = 0~0.15). Int J Appl Ceram Technol. 2018;00:1–7.

11. Kuang XJ, Xia HT, Liao FH, Wang CH, Li L, Jing XP, et al. Doping effects of Ta on conductivity and microwave dielectric loss of $MgTiO_3$ ceramics.J Am Ceram Soc.2007;90:3142-47.

12. Chen S, Li L, Yu S, Zheng H, Sun Z. High dielectric constant and high-Q in microwave ceramics of $SrTiO_3$ co-doped with aluminum and niobium. J Am Ceram Soc.2018 ;101:1835-40.

13. Jo HJ, Kim ES. Effects of structural characteristics on microwave dielectric properties of $MgTi_{1-x}(Mg_{1/3}B_{2/3})_xO_3$ (B = Nb, Ta). J Eur Ceram Soc.2016; 36:1399-1405.

14. Li L, Ren X, Liao Q. Crystal structure and microwave dielectric properties of $Zn_{0.9}Ti_{0.8-x}Sn_xNb_{2.2}O_8$ ceramics.Ceram Int.2012;38:3985-89.

15. Reaney IM, Colla EL, Setter N. Dielectric and structural characteristics of Ba- and Sr-based complex perovskites as a function of tolerance factor. Jpn J Appl Phys.1994;33:3984-90.

16. Hakki BW, Coleman PD. A dielectric resonant method of measuring inductive capacitance in the millimeter range. IRE Trans. Microwave Theory Tech.1960;8:402–10.

17. Fan XC, Chen XM, Liu XQ. Complex permittivity measurement on high Q materials via combined numerical approaches. IEEE Trans. Microwave Theory Tech. 2005;53[10]: 3130-34.

18. Nien CH, Lu HY, Tan X. Crystallographic orientation relationships between $SrTiO_3$ and Ruddlesden Popper Phase. J Am Ceram Soc.2011; 95:1676-81.

19. Ruddlesden SN, Popper P. The compound $Sr_3Ti_2O_7$ and its structure. Acta Crystallogr.1958;11: 54–55.

20. McCoy MA, Grimes RW, Lee WE. Phase stability and interfacial structures in the SrO–$SrTiO_3$ system. Philos Mag A.1997;75: 833-46.

21. Bacq OL, Salinas E, Pisch A, Pasturel A. First-principles structural stability in the strontium–titanium–oxygen system. Philos Mag. 2006; 86:2283-92.

22. Shannon RD. Revised effective ionic radii and systematic studies of interatomic distances in halides and chalcogenides. Acta Crystallogr.1976;A32:751–67.

23. Shannon RD, Rossman GR. Dielectric constants of silicate garnets and the oxide additivity rule, Am Mineral.1992;77:94-100.

24. Shannon RD. Dielectric polarizabilities of ions in oxides and fluorides. J Appl Phys.1993; 73:348-66.

25. Zhang T, Zuo R, Zhang J. Structure, microwave dielectric properties, and low-temperature sintering of acceptor/donor codoped $Li_2Ti_{1-x}(Al_{0.5}Nb_{0.5})_xO_3$ ceramics. J Am Ceram Soc.2016; 99:825-32.

26. Xiao M, Gu Q, Zhou Z, Zhang P. Study of the microwave dielectric properties of $(La_{1-x}Sm_x)NbO_4$ (x=0-0.10) ceramics via bond valence and packing fraction. J Am Ceram Soc.2017;100:3952-60.

27. Liu XC, Hong R, Tian C. Tolerance factor and the stability discussion of ABO_3-type ilmenite. J Mater Sci: Mater Electron.2009;20:323-27.

28. Liu X, Gao F, Tian C, Synthesis, low-temperature sintering and the dielectric properties of the ZnO-(1-x)TiO_2-xSnO_2(x=0.04–0.2). Mater Res Bull.2008;43:693-99.

29. Magrez A, Cochet M, Joubert O, Louarn G, Ganne M, Chauvet O. High internal stresses in $Sr_{1-x}La_{1+x}Al_{1-x}Mg_xO_4$ solid solution ($0 \leq x \leq 0.7$) characterized by infrared and raman spectroscopies coupled with crystal structure refinement. Chem Mater.2001;13:3893-98.

30. Pauling L. The nature of the chemical bond. IV. The energy of single bonds and the relative electronegativity of atoms. J Am Chem Soc. 1932;54:3570–82.

31. Brown ID, Shannon RD. Empirical bond-strength–bond-length curves for oxides. Acta Crystallogr.1973; A29:266-82.

32. Brown ID, Wu KK. Empirical parameters for calculating cation–oxygen bond valences. Acta Crystallogr.1976;B32:1957-59.

33. Park HS, Yoon KH, Kim ES. Relationship between the bond valence and the temperature coefficient of the resonant frequency in the complex perovskite $(Pb_{1-x}Ca_x)[Fe_{0.5}(Nb_{1-y}Ta_y)_{0.5}]O_3$.J Am Ceram Soc.2001;84:99-103.

34. Kim ES, Chun BS, Freer R, Cernik RJ. Effects of packing fraction and bond valence on microwave dielectric properties of $A^{2+} B^{6+} O_4$ (A^{2+}: Ca, Pb, Ba; B^{6+}: Mo, W) ceramics. J Eur Ceram Soc.2010;30:1731-36.

35. Jo HJ, Kim JS, Kim ES. Microwave dielectric properties of $MgTiO_3$-based ceramics. Ceram Int.2015;41:S530-S36.

36. Kim ES, Jeon CJ. Microwave dielectric properties of $ATiO_3$ (A= Ni, Mg, Co, Mn) ceramics. J Eur Ceram Soc.2010;30:341-46.

37. Chia CT, Chen YC, Cheng HF, Lin IN. Correlation of microwave properties and normal vibration mode of $xBa(Mg_{1/3}Ta_{2/3})O_3-(1-x)Ba(Mg_{1/3}Nb_{2/3})O_3$ Ceramics: I Raman spectroscopy. J Appl Phys.2003;94:3360-64.

38. Shi H, Fu Q, Wang G, Zhang L, Zheng Z, Luo W, et al. Microwave dielectric ceramics in $(Mg_{1/3}Sb_{2/3})O_2$-ZrO_2-TiO_2 system with near zero τ_f and low loss in a very wide range. Ceram Int.2018;44:19165-70.

39. Chen GY, Ren GR, Li L, Liu B, Chen XM. Structure and microwave dielectric properties of $SrLa[Al_{1-x}(Mg_{0.5}Ti_{0.5})_x]O_4$ (x= 0.2–0.8) ceramics. Ceram Int.2018;44:1984-90.

40. Ren GR, Zhu JY, Li L, Liu B, Chen XM. $SrLa(R_{0.5}Ti_{0.5})O_4$ (R=Mg,Zn) microwave dielectric ceramics with complex K_2NiF_4-type layered perovskite structure. J Am Ceram. Soc.2016;100:2582-2589.

41. Kawashima S, Nishida M, Ueda I, Ouchi H. Ba($Zn_{1/3}Ta_{2/3}$)O_3 ceramics with low dielectric loss at microwave frequencies. J Am Ceram Soc.1983;66:421-423.

42. Nomura S, Toyama K, Kaneta K. Ba($Mg_{1/3}Ta_{2/3}$)O_3 ceramics with temperature-stable high dielectric constant and low microwave loss. Jpn J Appl Phys.1982;21:L624-L626.

TABLE 1 Lattice parameters, tolerance factor *t*, and reliability factors of $Sr_2[Ti_{1-x}(Al_{0.5}Nb_{0.5})_x]O_4$ ceramics.

	***x*=0**	***x*=0.10**	***x*=0.25**	***x*=0.30**	***x*=0.50**
a(Å)	3.8856	3.8865	3.8873	3.88572	3.88574
c(Å)	12.5948	12.5977	12.6045	12.6026	12.6030
V[A^3]	190.15	190.29	190.46	190.28	190.29
R_p	7.14	7.76	8.55	8.13	7.97
R_{wp}	9.2	10.4	11.2	10.7	10.6
Rb	3.04	4.12	3.25	4.56	4.64
χ^2	3.5	3.7	3.98	5.15	5.02
t	0.9557	0.9565	0.9578	0.9580	0.9599

TABLE 2 Microwave dielectric properties of $Sr_2[Ti_{1-x}(Al_{0.5}Nb_{0.5})_x]O_4$ ceramics

Composition	ε_r	***Qf* (GHz)**	**τ_f (ppm/°C)**
x=0	42	11,2900	132
x =0.10	34.3	60,200	87
x =0.25	30	11,3000	48
x =0.30	30.2	83,960	37
x =0.50	25.1	77,580	14

TABLE 3. Dielectric constant ε_r , ionic dielectric polarizabilities α_{Theo}(Å^3) and calculated dielectric constant $\varepsilon_{r\ calc}$.

x	ε_r	$\alpha_{Theo.}$(Å^3)	$\varepsilon_{r\ calc}$
x=0	42	19.44	20.90
x =0.10	34.3	19.38	20.44
x =0.25	30	19.30	19.87
x =0.30	30.2	19.27	19.81
x =0.50	25.1	19.16	19.18

TABLE 4 Covalency of $Sr_2[Ti_{1-x}(Al_{0.5}Nb_{0.5})_x]O_4$ ceramics.

Compound		R(Å)	R$_1$	N	s	f_c	Covalency (%)	Average Covalency (%)
x=0	Sr-0	2.6852	2.143	7.0	0.206	0.0411	19.92	
	Ti-O	1.9615	1.806	5.20	0.651	0.2491	38.3	29.11
x =0.10	Sr-0	2.4791	2.143	7.0	0.361	0.0988	27.40	
	Ti-O	1.9552	1.806	5.20	0.662	0.2562	38.7	33.05
x =0.25	Sr-0	2.4553	2.143	7.0	0.386	0.1098	28.47	
	Ti-O	1.9629	1.806	5.20	0.648	0.255	38.7	33.59
x =0.30	Sr-0	2.4511	2.143	7.0	0.391	0.1119	28.67	
	Ti-O	1.9640	1.806	5.20	0.646	0.2470	38.2	33.44
x =0.50	Sr-0	2.4442	2.143	7.0	0.3983	0.1155	28.99	
	Ti-O	1.9661	1.806	5.20	0.642	0.2448	38.1	33.55

TABLE 5 Effective ionic radii r_A (Å), r_B (Å) r_o(Å), unit cell volume (V_{cell}), formula unit (Z), packing fraction (P.F.) of $Sr_2[Ti_{1-x}(Al_{0.5}Nb_{0.5})_x]O_4$ ceramics.

x	r_A (Å)	r_B (Å)	r_o(Å)	V_{cell}	Z	P.F
x=0	1.31	0.605	1.4	190.16	2	59.2361
x =0.10	1.31	0.603	1.4	190.29	2	59.1859
x =0.25	1.31	0.601	1.4	190.46	2	59.1205
x =0.30	1.31	0.600	1.4	190.28	2	59.1735
x =0.50	1.31	0.596	1.4	190.30	2	59.1492

TABLE 6 Microwave dielectrics of some typical materials with a dielectric constant around 25.

Materials	ε_r	Qf (GHz)	τ_f (ppm/°C)	Reference
$SrLa[Al_{1-x}(Mg_{0.5}Ti_{0.5})_x]O_4$	22.2	89,100	-0.1	39
$(Nd_{1-x}Bi_x)NbO_4$	22.5	50,000	-9	4
$(Mg_{1/3}Sb_{2/3})O_2$-ZrO_2-TiO_2	24.4	41,800	-4.6	38
$SrLa(Mg_{0.5}Ti_{0.5})O_4$	25.5	72,000	29	40
$SrLa(Zn_{0.5}Ti_{0.5})O_4$	29.4	34,000	38	40
$Ba(Zn_{1/3}Ta_{2/3})O_3$	29	168,000	0	41
$Ba(Mg_{1/3}Ta_{2/3})O_3$	25	176,400	2.7	42
$Sr_2[Ti_{0.75}(Al_{0.5}Nb_{0.5})_{0.25}]O_4$	30	11,3000	48	The present work
$Sr_2[Ti_{0.5}(Al_{0.5}Nb_{0.5})_{0.5}]O_4$	25.1	77,580	14	The present work

List of Figure Captions

FIGURE 1 XRD patterns for $Sr_2[Ti_{1-x}(Al_{0.5}Nb_{0.5})_x]O_4$ ceramics: (A) x = 0, (B) x = 0. 1, (C) x = 0.25, (D) x = 0.30, (E) x = 0.50.

FIGURE 2 Rietveld refinement patterns for $Sr_2[Ti_{1-x}(Al_{0.5}Nb_{0.5})_x]O_4$ ceramics for (A) x=0, (B) x=0.10 and (C) x=0.25.

FIGURE 3 Variation of unit cell volume of $Sr_2[Ti_{1-x}(Al_{0.5}Nb_{0.5})_x]O_4$ ceramics as a function of *x*.

FIGURE 4 Bulk density of $Sr_2[Ti_{1-x}(Al_{0.5}Nb_{0.5})_x]O_4$ ceramics as function of sintering temperature: (A) x = 0, (B) x = 0. 10, (C) x = 0.25, (D) x = 0.30, (E) x = 0.50.

FIGURE 5 SEM micrographs of polished and thermally etched surfaces of $Sr_2[Ti_{1-x}(Al_{0.5}Nb_{0.5})_x]O_4$ ceramics: (A) *x* = 0 sintered at 1600˚C, (B) *x* = 0. 1 sintered at 1600˚C, (C) *x* = 0.25 sintered at 1575 ˚C, (D) *x* = 0.30 sintered at 1575 ˚C, (E) *x* = 0.50 sintered at 1575 ˚C.

FIGURE 6 Variation *of* dielectric constant ε_r and theoretical dielectric polarizabilities α_{Theo}(Å^3). for $Sr_2[Ti_{1-x}(Al_{0.5}Nb_{0.5})_x]O_4$ ceramics.

FIGURE 7 Variation of tolerance factor of $Sr_2[Ti_{1-x}(Al_{0.5}Nb_{0.5})_x]O_4$ ceramics as a function of *x*.

FIGURE 8 Correlation between temperature coefficient τ_f and average degree of covalency (%) for $Sr_2[Ti_{1-x}(Al_{0.5}Nb_{0.5})_x]O_4$ ceramics as a function of *x*.

FIGURE 9 Variation tendency between *Qf* value and packing fraction (P.F) for $Sr_2[Ti_{1-x}(Al_{0.5}Nb_{0.5})_x]O_4$ ceramics as a function of *x*.

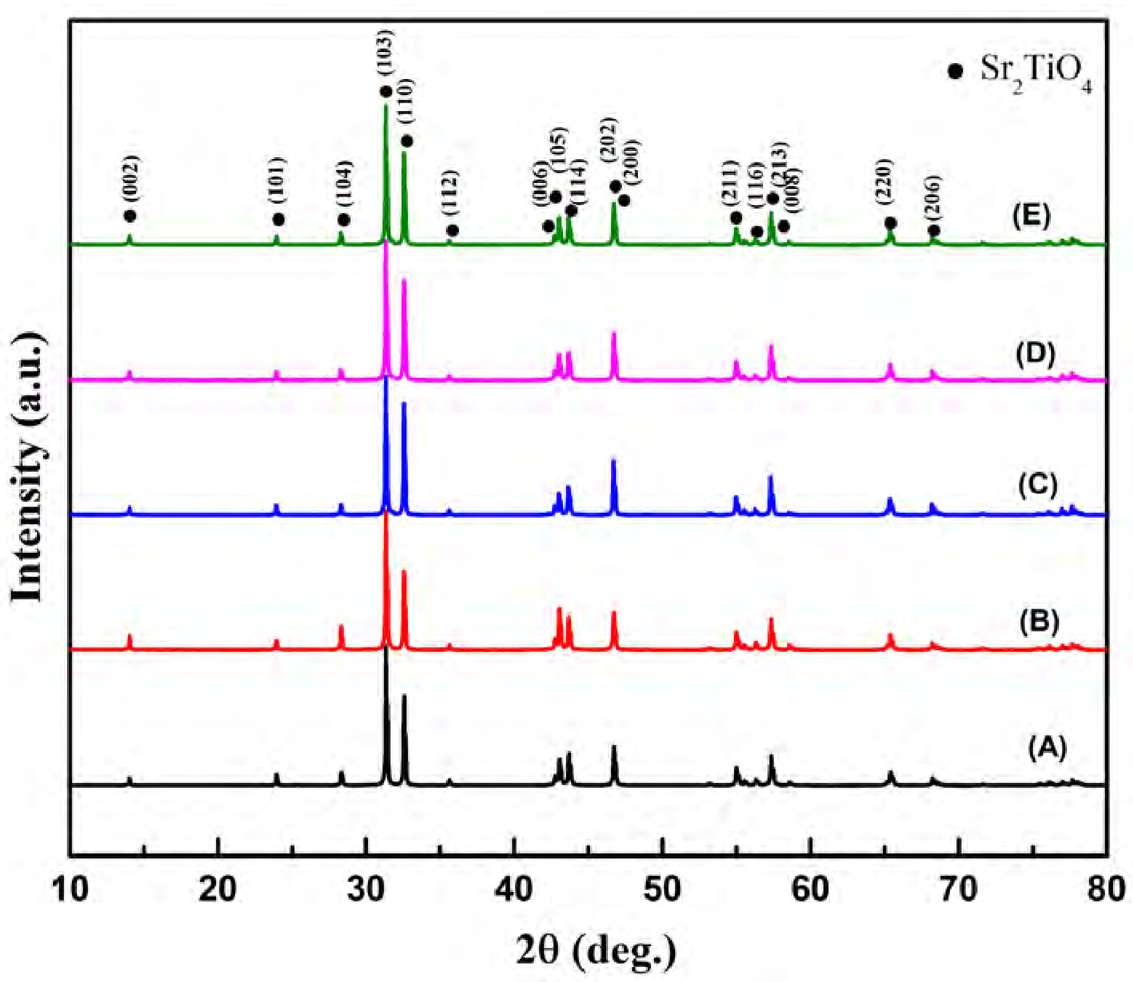
● Sr_2TiO_4
(002)
(101)
(104)
(103)
(110)
(112)
(006)
(105)
(114)
(202)
(200)
(211)
(116)
(213)
(008)
(220)
(206)
(E)
(D)
(C)
(B)
(A)
Intensity (a.u.)
10
20
30
40
50
60
70
80
2θ (deg.)

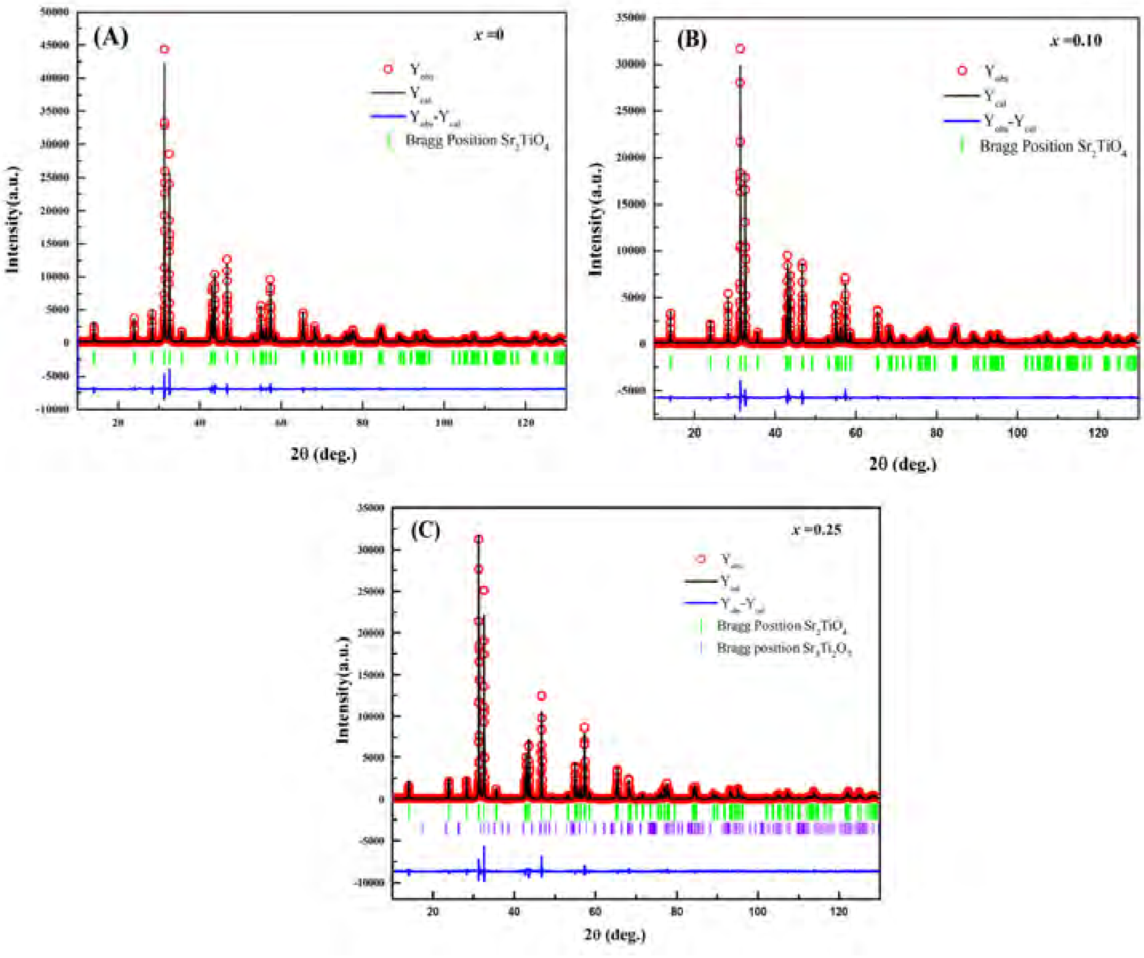
(A)
x =0
Y_obs
Y_cal
Y_obs-Y_cal
Bragg Position Sr2TiO4
Intensity(a.u.)
2θ (deg.)
(B)
x =0.10
Y_obs
Y_cal
Y_obs-Y_cal
Bragg Position Sr2TiO4
Intensity(a.u.)
2θ (deg.)
(C)
x =0.25
Y_obs
Y_cal
Y_obs-Y_cal
Bragg Position Sr2TiO4
Bragg position Sr3Ti2O7
Intensity(a.u.)
2θ (deg.)

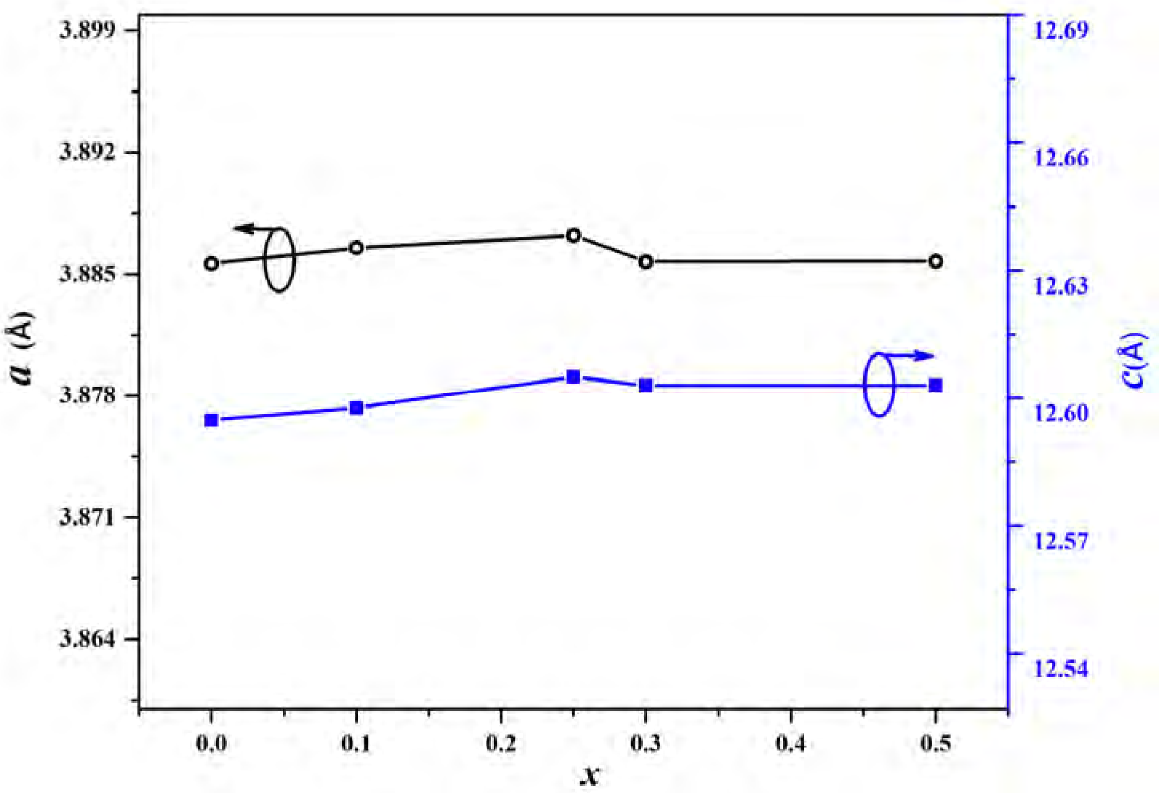
3.899
3.892
3.885
3.878
3.871
3.864
a (Å)
12.69
12.66
12.63
12.60
12.57
12.54
c (Å)
0.0
0.1
0.2
0.3
0.4
0.5
x

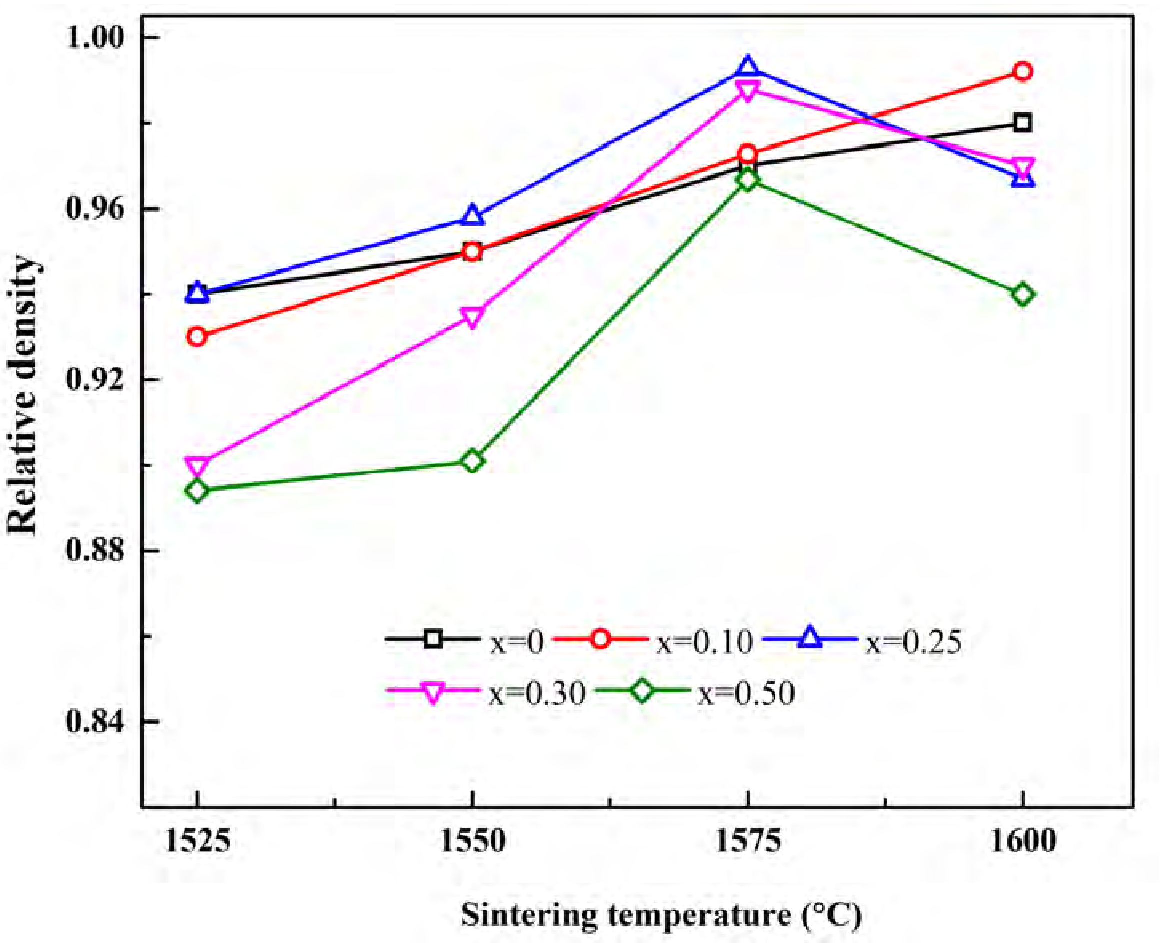
1.00
0.96
0.92
0.88
0.84
Relative density
1525
1550
1575
1600
Sintering temperature (°C)
x=0
x=0.10
x=0.25
x=0.30
x=0.50

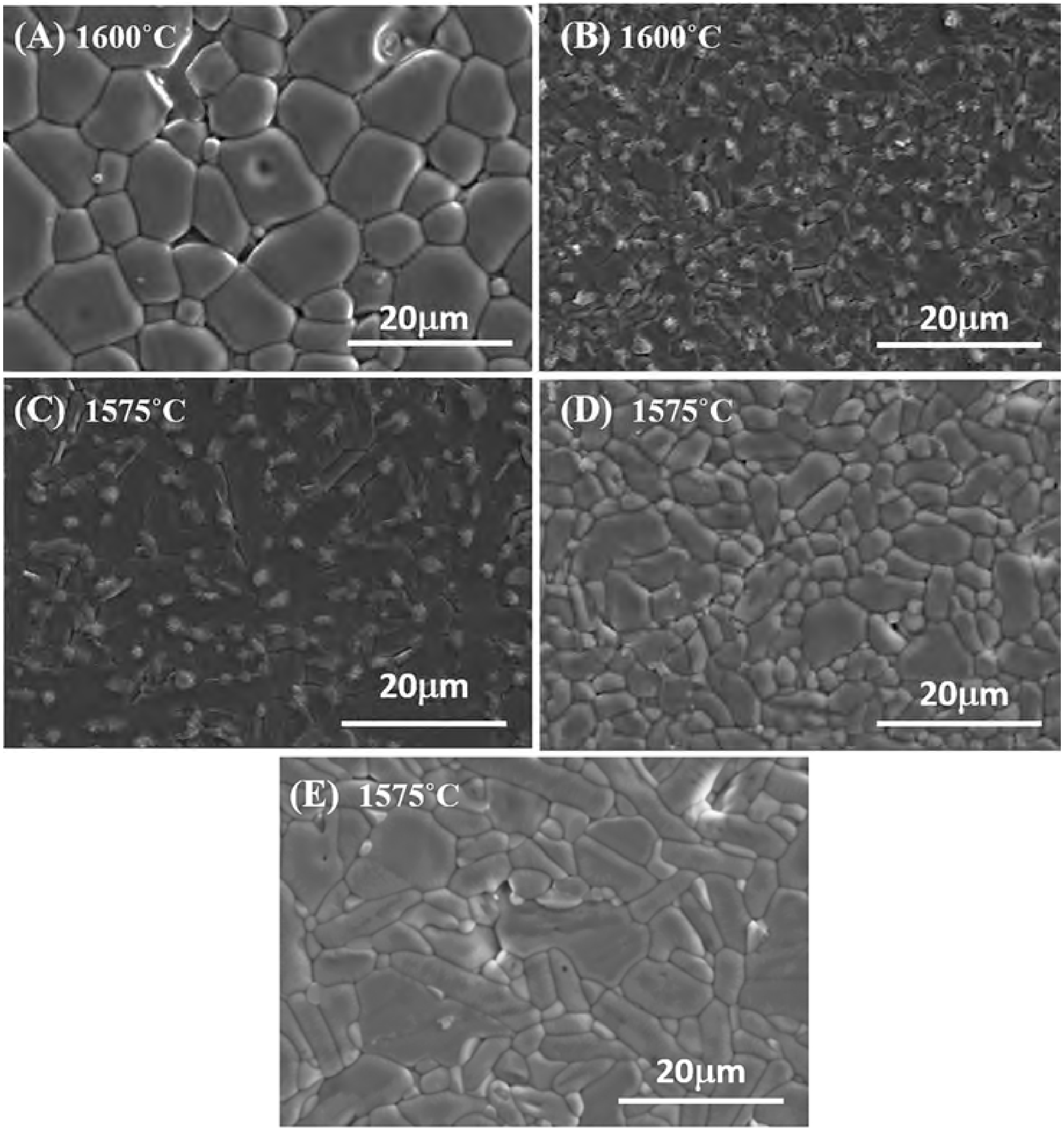
(A) 1600°C
20μm
(B) 1600°C
20μm
(C) 1575°C
20μm
(D) 1575°C
20μm
(E) 1575°C
20μm

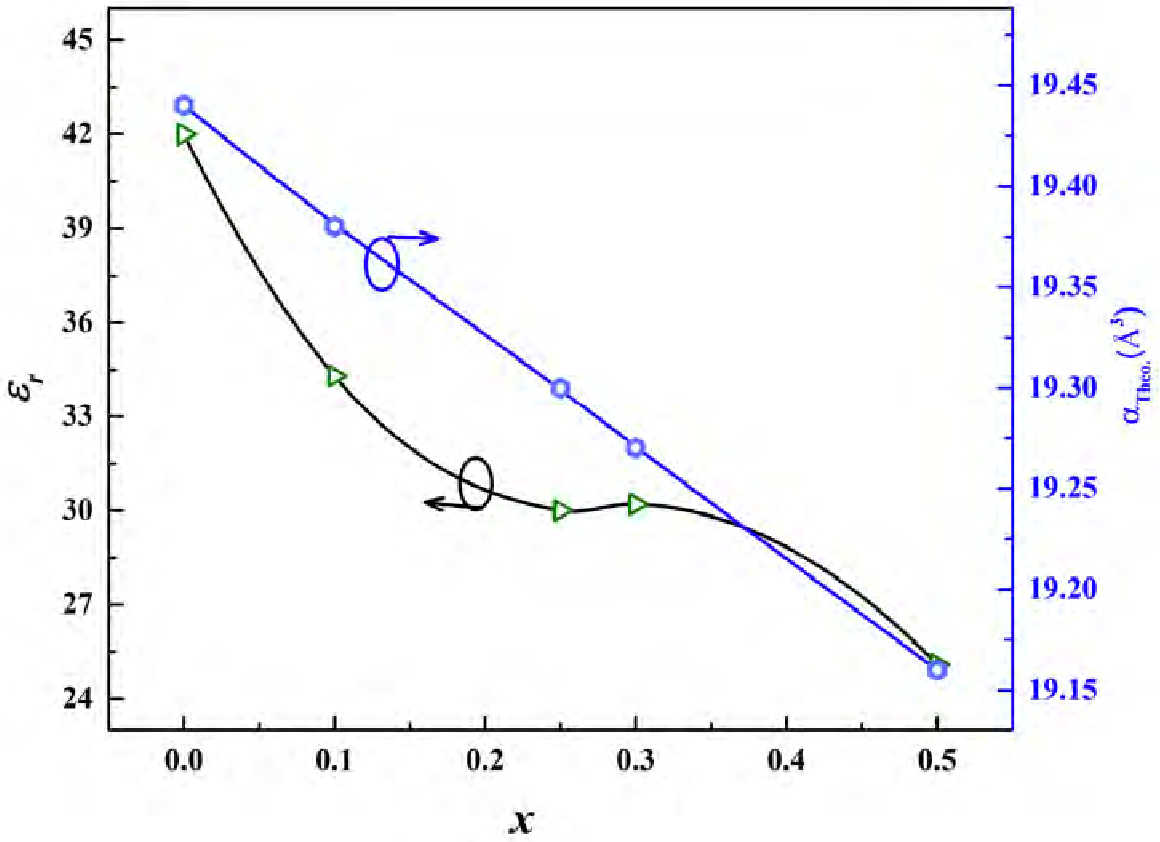
45
42
39
36
33
30
27
24
ε_r
0.0
0.1
0.2
0.3
0.4
0.5
x
19.45
19.40
19.35
19.30
19.25
19.20
19.15
$\alpha_{\mathrm{Theo.}}$ (Å^3)

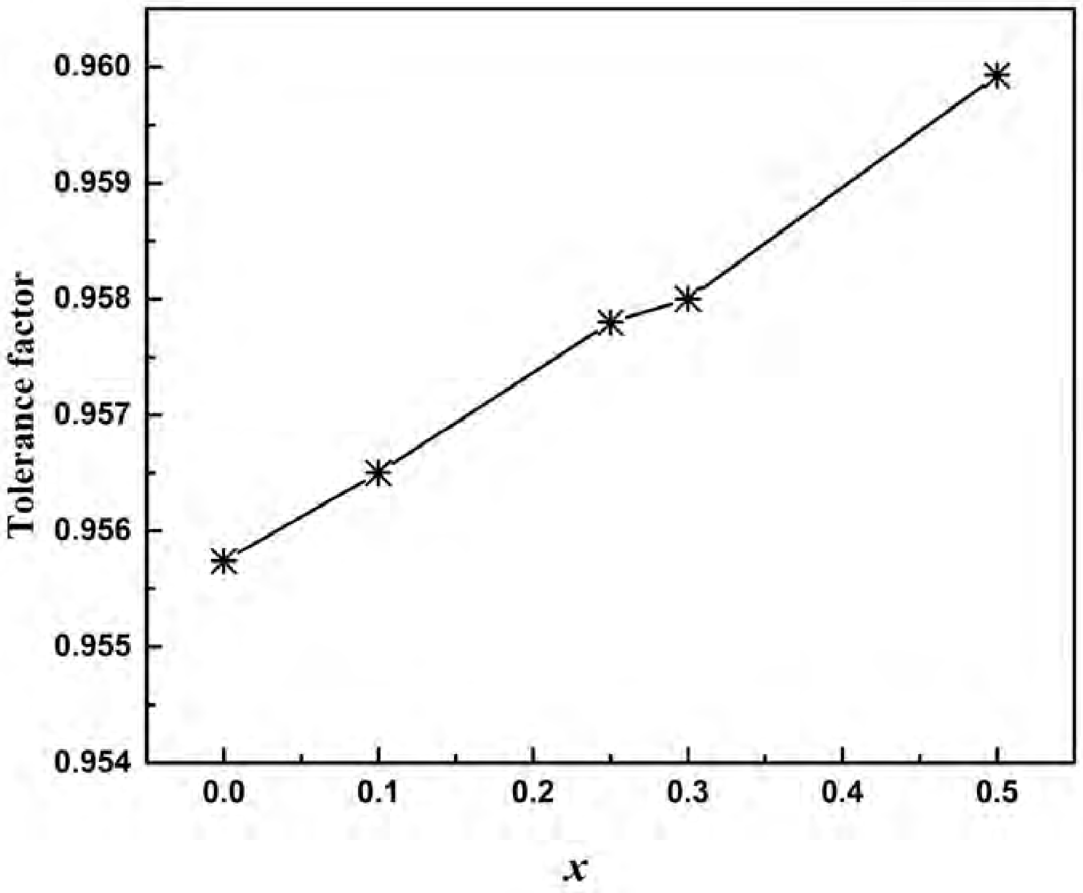
Tolerance factor
0.954
0.955
0.956
0.957
0.958
0.959
0.960
0.0
0.1
0.2
0.3
0.4
0.5
x

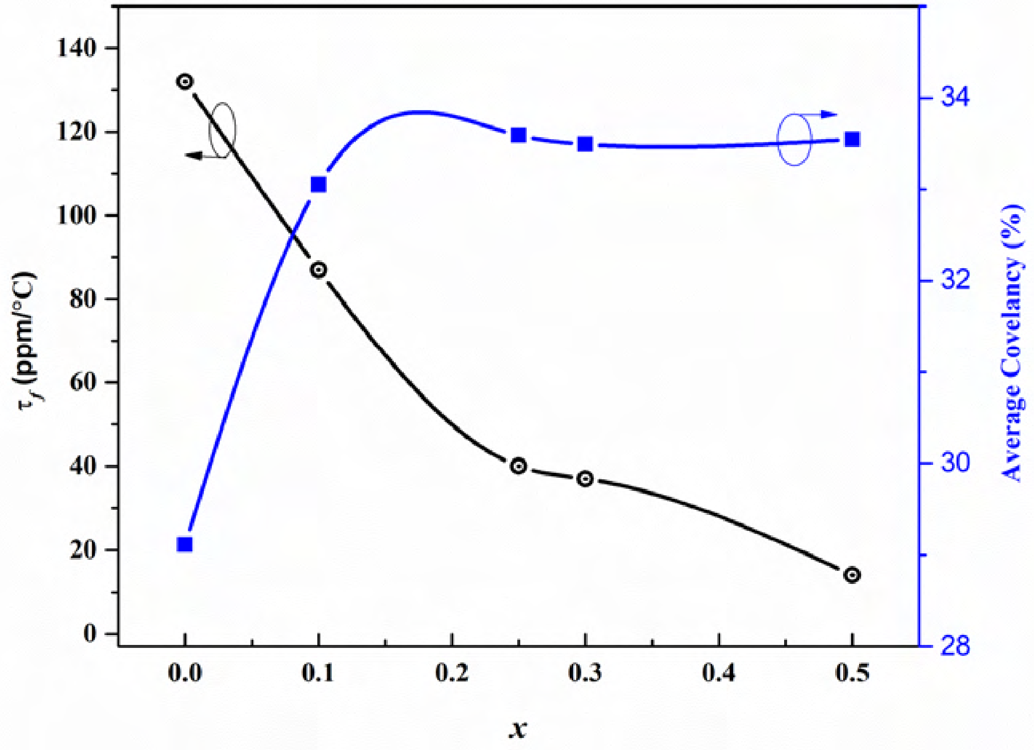

τ_f (ppm/°C)
140
120
100
80
60
40
20
0
0.0
0.1
0.2
0.3
0.4
0.5
x
34
32
30
28
Average Covelancy (%)

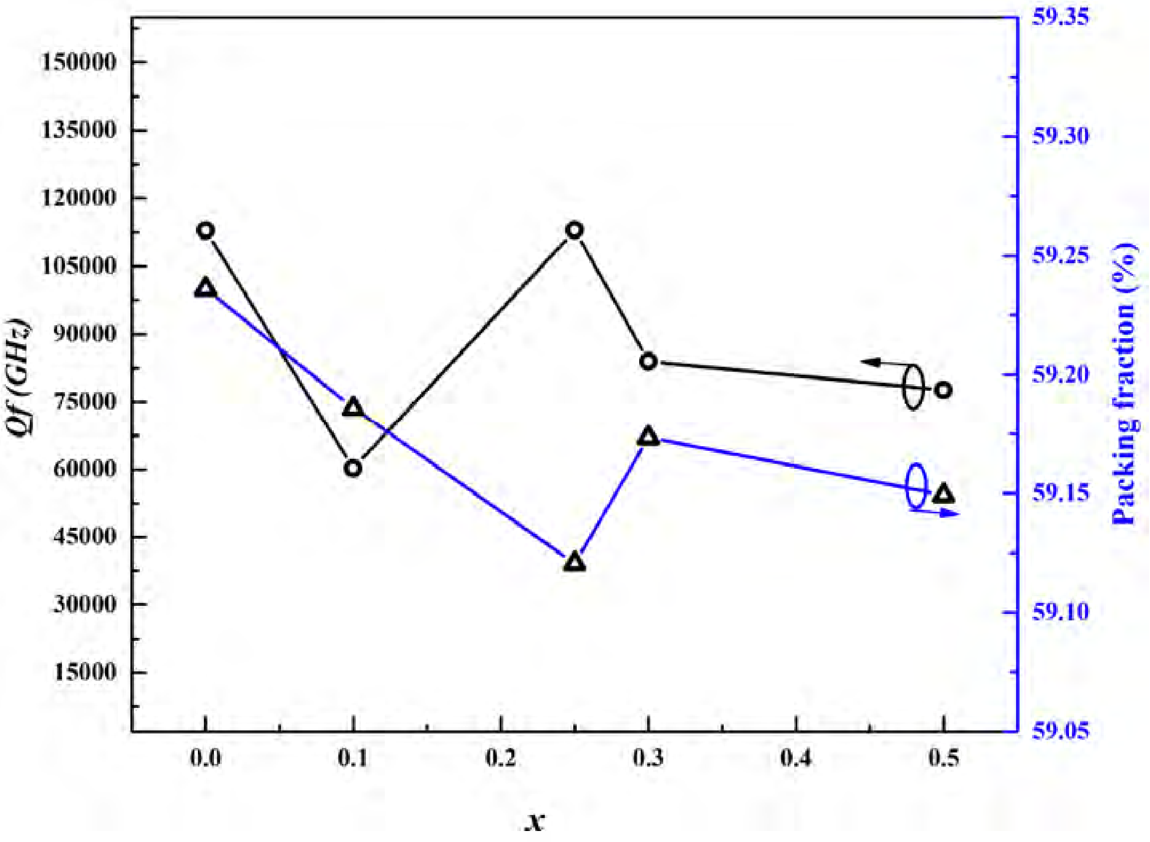
150000
135000
120000
105000
90000
75000
60000
45000
30000
15000
Qf (GHz)
59.35
59.30
59.25
59.20
59.15
59.10
59.05
Packing fraction (%)
0.0
0.1
0.2
0.3
0.4
0.5
x